

**FEED SPACER OF SPIRAL WOUND MEMBRANE MODULE FOR
NANOFILTRATION AND REVERSE OSMOSIS: MODELING,
SIMULATION AND DESIGN**

by

LAU KOK KEONG

**Thesis submitted in fulfillment of the
requirements for the degree of
Doctor of Philosophy**

FEBRUARY 2007

ACKNOWLEDGEMENTS

First of all, I would like to express my deepest gratitude to my parents Mr. Lau Kam Pooi and Madam Kong Chan Lan who encouraged me to pursue my PhD degree. Thank you for your persevering support and encouragement.

My sincere thanks to both of my supervisors, Prof. Abdul Latif Ahmad and Assoc. Prof. Dr. Mohamad Zailani Abu Bakar for their prestigious guidance and supervision as well as their effort in the coordination of this research project until the completion of this thesis.

I wish to show my grateful thanks to MOSTI for providing me the NSF scholarship. Besides, I would also like to express my heart-felt gratitude to all the laboratory technicians particularly Mr. Shaharin Mohamed, Mr. Osmarizal Osman, Mr. Syamsul Hidayat, Mr., Mohd. Roqib Rashidi, Mr. Said Saidin and Mrs. Latiffah Latif for their assistance. My appreciation also goes to Pn. Hasnah Hassan , Pn. Aniza Abdul Ghani, Pn. Azni Shahida Khalid and Cik Badilah Baharom.

On top of that, I would like to express my appreciation to Esther Liew for giving me fully support and dedication and Mei Fong for sharing so much knowledge with me. Special thanks also to Boon Seng, Siew Chun, Choi Yee, Lian See, Siang Piao, Derek, Ramesh, Yin Fong, Pei Ching, Kelly, Ivy Tan, Cheng Teng, Jia Huey, Foo, Sam and Mook Tzeng for their friendship spirit. Last but not least, I would like to thank MOSTI for funding this research through IRPA R&D grant.

LAU KOK KEONG

FEBRUARY 2007

TABLE OF CONTENTS

	Page
ACKNOWLEDGEMENTS	ii
TABLE OF CONTENTS	iii
LIST OF TABLES	ix
LIST OF FIGURES	xi
LIST OF PLATES	xxi
LIST OF SYMBOLS	xxii
LIST OF ABBREVIATIONS	xxvi
ABSTRAK	xxvii
ABSTRACT	xxvix

CHAPTER ONE : INTRODUCTION

1.1	Membrane processes	1
1.2	Membrane module	4
	1.2.1 Plate-and-frame module	4
	1.2.2 Tubular module	5
	1.2.3 Hollow fiber module	5
	1.2.4 Spiral wound module	7
1.3	Membrane module market demand	8
1.4	Advantages in spiral wound membrane	10
1.5	Problem statement	11
1.6	Project objectives	15
	1.6.1 Main objective	15
	1.6.2 Measurable objectives	15
1.7	Scope of research project	16
1.8	Organization of the thesis	18

CHAPTER TWO : LITERATURE REVIEW

2.1	Construction and material of spiral wound membrane module	21
	2.1.1 Permeate collection tube	23

2.1.2	Permeate spacer	24
2.1.3	Feed Spacer	24
2.1.4	Anti-telescoping device (ATD)	25
2.1.5	Interconnector	25
2.1.6	Outer wrap	26
2.2	Concentration polarization and fouling in spiral wound membrane feed channel	27
2.2.1	Concentration polarization	27
2.2.2	Fouling mechanisms that contributed by concentration polarization	30
2.2.2(a)	Gel polarization	30
2.2.2(b)	Adsorption of solute	31
2.2.2(c)	Scaling of solute	32
2.2.3	Others fouling problem in spiral wound membrane module	34
2.2.4	Common methods to control fouling problem in spiral wound membrane module	34
2.3	Feed spacer	36
2.3.1	Type of construction	38
2.3.2	Type of spacer configuration	39
2.3.3	Spacer design parameters	42
2.3.4	Commercial feed spacer	44
2.4	Feed spacer design	47
2.4.1	Hydrodynamics and mass transfer in empty SWM feed channel	47
2.4.2	Hydrodynamics and mass transfer in spacer filled SWM feed channel	49
2.4.3	Design by experimental method	50
2.4.4	Design by Computational Fluid Dynamics (CFD) method	56
2.4.4(a)	Design by Computational Fluid Dynamics simulation (CFD) method	57
2.4.4(b)	Design by Computational Fluid Dynamics (CFD) mathematical modeling	60
2.4.4(c)	Design by Computational Fluid Dynamics (CFD) simulation integrated with permeation properties	64
2.5	Summary	65

CHAPTER THREE : MATERIALS AND METHODS

3.1	Modeling and simulation method	71
3.1.1	Computational domain and governing equations	71
3.1.1(a)	Governing equations for 2-D incompressible flow model	72
3.1.1(b)	Governing equations for 3-D incompressible flow model	73
3.1.2	Discretization and solution of governing equations	74
3.1.2(a)	Discretization of momentum equation	75
3.1.2(b)	Discretization of continuity equation	76
3.1.2(c)	Pressure-velocity coupling (SIMPLE algorithm)	78
3.1.2(d)	Discretization scheme	79
3.1.2(e)	Algebraic multigrid (AMG)	80
3.1.2(f)	Solution method	81
3.1.3	Permeation properties modeling	82
3.1.3(a)	Membrane transport model	83
3.1.3(b)	Modified film theory	86
3.1.4	Simulation approach	88
3.1.4(a)	Direct Simulation (DS)	88
3.1.4(b)	Periodic Unit Cell Simulation (PUCS)	88
3.1.4(c)	Permeation Properties Integrated Simulation (PPIS)	91
3.1.5	Boundary condition and User-Defined Function (UDF)	93
3.1.5(a)	Boundary condition for empty SWM membrane channel	93
3.1.5(b)	Boundary condition for 2-D spacer filled SWM channel	95
3.1.5(c)	Boundary condition for 3-D spacer filled SWM channel	97
3.1.5(d)	User-Defined Scalar (UDS) and User-Defined Function (UDF) for PPIS	99
3.1.6	Simulation condition	101
3.1.6(a)	Feed solution system	101
3.1.6(b)	Simulation domain for spacers with different design parameters	102
3.1.6(c)	Simulation test	108

3.1.7	Computational grid generation and optimization	112
3.1.7(a)	Narrow empty membrane channel	112
3.1.7(b)	2-D spacer filled SWM channel	113
3.1.7(c)	3-D spacer filled SWM channel	113
3.1.7(d)	Grid size optimization	115
3.1.8	Validation approach for integrated CFD model	117
3.2	Experimental method	119
3.2.1	Experimental set-up	119
3.2.1(a)	Membrane permeation test cell	119
3.2.1(b)	Membrane permeation test rig	121
3.2.2	Material	123
3.2.2(a)	Feed solution	123
3.2.2(b)	Type of membrane	123
3.2.2(c)	Fabrication of feed spacer	123
3.2.3	Experimental procedures and analytical method	126
3.2.3(a)	Experimental procedures and analytical method for integrated model validation	126
3.2.3 (b)	Experimental procedures for spacer performance comparison	128

CHAPTER FOUR : RESULTS AND DISCUSSIONS

4.1	Hydrodynamic and permeation properties studies for empty spiral wound membrane channel	131
4.1.1	Evaluation of membrane intrinsic properties	131
4.1.2	Integrated CFD model validation	133
4.1.3	Influence of permeation properties on membrane concentration prediction	138
4.1.4	Effect of feed Reynolds number on concentration polarization factor and mass transfer coefficient	142
4.1.5	Effect of transmembrane pressure on concentration polarization factor	144
4.1.6	Effect of different solutes on concentration polarization factor	145
4.2	Hydrodynamic and permeation properties studies for spacer filled spiral wound membrane feed channel	150

4.2.1	Integrated CFD model validation	150
4.2.2	Unsteady hydrodynamics analysis for spacer filled SWM feed channel	153
4.2.2(a)	Unsteady entrance transition effect in spacer filled SWM feed channel	155
4.2.2(b)	Effect of different spacer geometry on unsteady hydrodynamics	162
4.2.2(c)	Effect of different mesh length on unsteady hydrodynamics	164
4.2.2(d)	Effect of different mesh angle on unsteady hydrodynamics	167
4.2.2(e)	Effect of different spacer filament ratio on unsteady hydrodynamics	173
4.2.2(f)	Specific power consumption for different spacer filled membrane channel	174
4.2.3	Influence of unsteady hydrodynamics on concentration factor	178
4.2.3(a)	Wall shear stress analysis	178
4.2.3(b)	Development of concentration polarization under unsteady hydrodynamics in spacer filled membrane channel	186
4.3	Design and optimization of feed spacer	189
4.3.1	Spacer filament geometry design and optimization	194
4.3.1(a)	Design and optimization based on minimum Ψ	194
4.3.1(b)	Velocity contour plot study	195
4.3.1(c)	Wall shear stress analysis	197
4.3.1(d)	Localized concentration polarization factor study	199
4.3.2	Spacer mesh length ratio design and optimization	201
4.3.2(a)	Design and optimization based on minimum Ψ	202
4.3.2(b)	Velocity contour plot study	204
4.3.2(c)	Wall shear stress analysis	206
4.3.2(d)	Localized concentration polarization factor study	208
4.3.3	Spacer mesh angle design and optimization	212
4.3.3(a)	Design and optimization based on minimum Ψ	212
4.3.3(b)	Localized wall shear stress and concentration factor study	214

4.3.3(c) Wall shear stress analysis	221
4.3.4 Spacer filament ratio design and optimization	224
4.3.4(a) Design and optimization based on minimum Ψ	225
4.3.4(b) Localized wall shear stress and concentration factor study	226
4.3.4(c) Wall shear stress analysis	230
4.3.5 Model validation and performance comparison for optimum spacer	233
CHAPTER FIVE : CONCLUSIONS AND RECOMMENDATIONS	
5.1 Conclusions	238
5.2 Recommendations	242
BIBLIOGRAPHY	244
APPENDICES	
Appendix A Samples of User Defined Function (UDF)	257
Appendix B Photographic figure for experimental setup	267
Appendix C Average specific power consumption for different spacer designs	270
LIST OF PUBLICATIONS, SEMINAR AND AWARDS	271

LIST OF TABLES

		Page
Table 1.1	Membrane processes based on the mechanism of separation	1
Table 1.2	Characteristics of major membrane module designs	10
Table 1.3	Foulants and their control strategies in spiral wound module for nanofiltration and reverse osmosis processes	12
Table 1.4	Comparison of different CFD approaches to model SWM feed channel	14
Table 2.1	Material for permeate collection tube	23
Table 2.2	Fouling control methods for spiral wound module	35
Table 2.3	Spacer design parameters for some of available commercial feed spacers	45
Table 2.4	CFD commercial simulation packages	57
Table 2.5	Feed spacer design approaches	68
Table 3.1	Transport Properties for different types of solutes	102
Table 3.2	Simulated feed spacers for unsteady hydrodynamics analysis and spacer design optimization	103
Table 3.3	Overall Simulation test	109
Table 3.4	Simulation test for Integrated CFD Model validation	110
Table 3.5	Experimental permeation tests for CFD model validation	127
Table 4.1	Content summary for chapter results and discussions	130
Table 4.2	Curve-fitted Spiegler-Kedem parameters at feed concentration	133
Table 4.3	Schmidt number and osmotic pressure for different types of solutions at feed concentration	137
Table 4.4	Mean velocity magnitude and RMS of velocity magnitude fluctuation generated by spacers with different mesh length ratio (ML) in the SWM channel under Re_f 200 to 700	166
Table 4.5	Mean velocity magnitude and RMS of velocity magnitude fluctuation generated by spacers with different mesh angle (α and β) in the SWM channel under Re_f 100 to 600	172

Table 4.6	Mean velocity magnitude and RMS of velocity magnitude fluctuation generated by spacers with different filament ratio in the SWM channel under Re_f 100 to 450	174
Table 4.7	Spacer design variables and study range for the optimization of feed spacer	191
Table 4.8	Effective concentration polarization Factor, Ψ for different spacer filaments	195
Table 4.9	Effective time-distance averaged wall shear stress, $\overline{\tau_e}$ and effective RMS of distance averaged wall shear stress fluctuation, $\overline{\tau_e}'_{\text{RMS}}$ generated by different spacer filaments	198
Table 4.10	Effective time-distance averaged wall shear stress, $\overline{\tau_e}$ and effective RMS of distance averaged wall shear stress fluctuation, $\overline{\tau_e}'_{\text{RMS}}$ generated by spacer with different mesh length ratio (ML)	208
Table 4.11	Effective time-area averaged wall shear stress, $\overline{\tau_e}$ and effective RMS of area averaged wall shear stress fluctuation, $\overline{\tau_e}'_{\text{RMS}}$ generated by spacer with different mesh angle	223
Table 4.12	Effective time-area averaged wall shear stress, $\overline{\tau_e}$ and effective RMS of area averaged wall shear stress fluctuation, $\overline{\tau_e}'_{\text{RMS}}$ generated by spacer with different filament ratio (SFR)	232
Table 4.13	Study range and final optimum design parameters for feed spacer	233
Table 4.14	Experimental performance comparison for spacers with different designs	236
Table C.1	Average specific power consumption for spacers with different filaments geometries under Re_f 100 - 500	270
Table C.2	Average specific power consumption for spacers with different mesh length ratio under Re_f 200 - 600	270
Table C.3	Average specific power consumption for spacers with different mesh angles under Re_f 100 - 400	270
Table C.4	Average specific power consumption for spacers with different filament ratio under Re_f 100 - 260	270

LIST OF FIGURES

	Page	
Figure 1.1	Plate-and-frame membrane module	4
Figure 1.2	Tubular membrane module	5
Figure 1.3	Hollow fiber module with closed-end design	6
Figure 1.4	Hollow fiber module with opened-end design	6
Figure 1.5	Spiral Wound Membrane Module	7
Figure 1.6	World membrane market at 2009	9
Figure 2.1	Membrane envelope (leaf)	22
Figure 2.2	Spiral wound module: (a) basic element; leaves connected to a permeate tube, feed spacers between leaves; (b) leaves wound around permeate tube; (c) flows paths in SWM	22
Figure 2.3	Important parts for spiral wound membrane in pressure vessel	23
Figure 2.4	Concentration polarization phenomenon in membrane channel	27
Figure 2.5	Formation of gel layer on the membrane pore and surface	30
Figure 2.6	Formation of scale on the membrane surface due to concentration polarization layer	33
Figure 2.7	The formation of unsteady vortices (red circled areas) in porous feed spacer SWM channel	37
Figure 2.8	Type of feed spacer construction (a) Non-woven (b) Woven (c) Channel mesh	38
Figure 2.9	Type of feed spacer configuration (a) Ladder (b) Diamond	40
Figure 2.10	Contour plot for the transversal vortex in ladder spacer	41
Figure 2.11	Contour plot for the transversal and longitudinal vortex in diamond spacer	41
Figure 2.12	Feed spacer design parameters	42
Figure 2.13	Spacer with different number of filaments' layer (a) 2 layers spacer (b) Multiple layers spacer	44
Figure 3.1	Summary of overall research methods	70

Figure 3.2	Control volume used for discretization of governing equations	77
Figure 3.3	The segregated solution methods	82
Figure 3.4	Definition for δ_c in modified film theory	87
Figure 3.5	3-D Periodic Unit Cell Simulation (PUCS) (a) Spiral wound membrane feed spacer (b) 3-D Unit cell from plane view (c) 3-D Unit cell from Front view	89
Figure 3.6	Example of a periodic geometry	90
Figure 3.7	Periodic Unit Cell Simulation (PUCS) and Permeation Properties Integrated Simulation (PPIS)	92
Figure 3.8	Compensation of imbalanced mass in Single Cell Permeation Properties Integrated Simulation (SPPIS)	93
Figure 3.9	Boundary conditions for empty membrane channel	94
Figure 3.10	Boundary conditions for 2-D PUCS	95
Figure 3.11	Boundary condition for Multiple Cells Permeation Properties Integrated Simulation (MPPIS)	95
Figure 3.12	Boundary conditions for Unit Cell Simulation (PUCS)	97
Figure 3.13	Boundary conditions for Single Cell Permeation Properties Integrated Simulation (SPPIS)	98
Figure 3.14	Access of solver data by UDF for a single iteration loop	101
Figure 3.15	Computational domain for spacer filament geometry analysis	104
Figure 3.16	Computational domain for spacer mesh length ratio (ML) analysis	105
Figure 3.17	Computational domain for spacer mesh angle analysis ($\alpha = 90^\circ$)	106
Figure 3.18	Computational domain for spacer mesh angle analysis ($\alpha = 120^\circ$)	107
Figure 3.19	Computational domain for spacer mesh angle analysis ($\alpha = 30^\circ$)	107
Figure 3.20	Computational domain for spacer filament ratio analysis	108
Figure 3.21	Computational grid for empty membrane channel	112
Figure 3.22	2-D Computational grid for spacer filled SWM channel	113

Figure 3.23	3-D computational grid for spacer filled SWM channel (a) 2-D side view (x-direction) (b) 2-D side view (z-direction) (c) 3-D side view	114
Figure 3.24	Preliminary simulation test of optimum grid resolution for 2-D empty membrane channel (N_c = Number of cell, Re_f = 300, velocity magnitude for a vertical sampling line in middle of channel length)	115
Figure 3.25	Preliminary simulation test of optimum grid resolution for 2-D SWM spacer filled membrane channel (N_c = Number of cell, Re_f = 300, mean velocity magnitude for a vertical sampling line between 2 spacer filaments)	116
Figure 3.26	Preliminary simulation test of optimum grid resolution for 3-D unsteady hydrodynamics in SWM spacer filled membrane channel (N_c = Number of cell, Re_f = 500, mean velocity magnitude for a vertical yz surface between spacer filaments)	116
Figure 3.27	Calculation loop for integrated CFD model validation	118
Figure 3.28	Cross-sectional drawing for membrane permeation test cell	120
Figure 3.29	Schematic diagram for experimental set-up	122
Figure 4.1	Curve-fitting of Spiegler-Kedem parameters for various types of solutions (a) $MgSO_4$ (0.5%w/w) (b) Sucrose (0.2%w/w) (c) Na_2SO_4 (0.2%w/w)	132
Figure 4.2	Comparison between simulated and experimental data for $MgSO_4$ solution (0.5% w/w) (a) Low feed Reynolds number study (Re_f 320) (b) High feed Reynolds number study (Re_f 1200)	134
Figure 4.3	Comparison between simulated and experimental data for sucrose solution (0.2% w/w) (a) Low feed Reynolds number study (Re_f 320) (b) High feed Reynolds number study (Re_f 1200)	135
Figure 4.4	Comparison between simulated and experimental data for Na_2SO_4 solution (0.2% w/w) (a) Low feed Reynolds number study (Re_f 320) (b) High feed Reynolds number study (Re_f 1200)	136
Figure 4.5	Different types of permeation flux as boundary condition in membrane channel modeling	138

Figure 4.6	Evolution of predicted permeation flux along the membrane channel for MgSO ₄ under low feed Reynolds Number	139
Figure 4.7	Comparison of membrane concentration polarization factor (Γ) predicted by zero, constant and varying permeation flux modeling for MgSO ₄ (0.5%) solution under feed Reynolds number 320	140
Figure 4.8	Comparison of constant and varying permeation flux along the membrane channel for MgSO ₄ under feed Reynolds Number (Re_f) 320	141
Figure 4.9	Evolution of concentration factor under different feed Reynolds number for sucrose solution (0.2% w/w)	142
Figure 4.10	Evolution of mass transfer coefficient (k) under different feed Reynolds number for sucrose solution (0.2% w/w)	144
Figure 4.11	Evolution of concentration polarization factor, Γ along the membrane channel under different transmembrane pressure for sucrose solution (0.2% w/w)	145
Figure 4.12	Membrane wall transport properties for different solutions (a) MgSO ₄ (0.2% w/w) (b) Sucrose (0.2 %w/w) (c) Na ₂ SO ₄ (0.2% w/w)	146
Figure 4.13	Membrane wall Schmidt Number, Sc_w for various solutions (a) MgSO ₄ (0.2% w/w) (b) Sucrose (0.2% w/w) (c) Na ₂ SO ₄ (0.2% w/w)	148
Figure 4.14	Evolution of concentration polarization factor, Γ along the empty membrane channel for different solutions (0.2% w/w) under $\Delta P = 7$ bar	148
Figure 4.15	Comparison of simulated and experimental channel pressure drop for different types of spacer filled membrane channels	150
Figure 4.16	Comparison of simulated and experimental permeation fluxes for different types of spacer filled membrane channels under different pressure at feed Reynolds number 350 (a) Spacer ML1.5 - $\alpha 90\beta 0$ (b) ML3 -Spacer $\alpha 90\beta 0$ (c) Spacer ML6- $\alpha 90\beta 0$	152
Figure 4.17	Geometrical view (a-b) and the example of contour plot (c-d) for 2-D spacer filled SWM channel	154
Figure 4.18	Geometrical view (a-c) and the example of contour plot (d-e) for 3-D spacer filled SWM channel	155

Figure 4.19	2D contour plot of velocity magnitude in upstream spacer-filled membrane channel for a period of simulation time	156
Figure 4.20	2D velocity contour plot of unsteady hydrodynamics in downstream cylindrical spacer filled membrane channel for a period of simulation time	157
Figure 4.21	Instantaneous membrane wall shear stress along the membrane channel length generated by different spacer filament at $Re_f = 400$, $ML = 4$ (a) Cylindrical filament (b) Rectangular filament (c) Hexagonal filament	159
Figure 4.22	Instantaneous membrane wall shear stress along the membrane channel length generated by different mesh length ratio (ML 2-7) at Re_f 600 (a) ML 2 (b) ML 3 (c) ML 4 (d) ML 5 (e) ML 6 (f) ML 7	161
Figure 4.23	Development of unsteady hydrodynamics under different feed Reynolds number (Re_f) generated by cylindrical filament (a) Re_f 50 – Re_f 200 (b) Re_f 300 – Re_f 500	162
Figure 4.24	Development of unsteady hydrodynamics under different feed Reynolds number (Re_f) generated by rectangular filament (a) Re_f 50 – Re_f 200 (b) Re_f 300 – Re_f 500	163
Figure 4.25	Development of unsteady hydrodynamics under different feed Reynolds number (Re_f) generated by hexagonal filament (a) Re_f 50 – Re_f 200 (b) Re_f 300 – Re_f 500	163
Figure 4.26	Fluctuation of velocity magnitude generated by spacers with mesh length ratio ML 2-7 at feed Reynolds number, $Re_f = 500$ (a) ML 2 - ML4 (b) ML 5 - ML7	167
Figure 4.27	Evolution of unsteady vortices in the 3D spacer filled membrane channel	168
Figure 4.28	Unsteady vortices in the 3D spacer filled membrane channel at simulation time 1.0 s (Plane view, Spacer $\alpha=90^\circ$, $ML=3$, membrane walls have been removed from view, sampling at horizontal x-z contour surface, $y=0.5$ mm) (a) $\beta = 0^\circ$ (b) $\beta = 15^\circ$ (c) $\beta = 30^\circ$ (d) $\beta = 45^\circ$	169
Figure 4.29	Unsteady vortices in the 3D spacer filled membrane channel at simulation time 1.0 s (Plane view, Spacer $\alpha=120^\circ$, $ML=3$, membrane walls have been removed from view) (a) $\beta = 0^\circ$ (b) $\beta = 30^\circ$ (c) $\beta = 60^\circ$	170

Figure 4.30	Unsteady vortices in the 3D spacer filled membrane channel at simulation time 1.0 s (Plane view, Spacer $\alpha=30^\circ$, ML = 3, membrane walls have been removed from view, sampling at horizontal x-z contour surface, $y=0.5$ mm) (a) $\beta = 0^\circ$ (b) $\beta = 15^\circ$	170
Figure 4.31	Definition for spacer filament ratio and secondary flow	173
Figure 4.32	Specific power consumption generated by different types of spacer filaments Re_f 100 to 500	175
Figure 4.33	Specific power consumption generated by spacers with different mesh length ratio under Re_f 200 to 600	176
Figure 4.34	Specific power consumption generated by spacers with different mesh angle under Re_f 100 to 400	176
Figure 4.35	Specific power consumption generated by spacers with different filament ratios (SFR) under Re_f 100 to 400	177
Figure 4.36	Comparison of experimental permeation flux generated by empty and spacer filled membrane	178
Figure 4.37	Evolution of concentration factor and instantaneous wall shear stress along the membrane wall at simulation time 1.0000s (2-D simulation, Feed solution = CuSO_4 2%, Cylindrical spacer ML4, $Re_f = 400$) (a) Location of stagnant zones (b) Membrane located adjacent to the spacer (c) Membrane located opposite to the spacer	180
Figure 4.38	Contour plot of membrane wall shear stress and concentration in spacer filled membrane channel at simulation time 1.0000s (Feed solution = CuSO_4 2%, spacer ML3- $\alpha 90^\circ \beta 0$, circled regions indicate the stagnant zones, $Re_f = 100$)	182
Figure 4.39	Contour plot of membrane wall shear stress and concentration in spacer filled membrane channel at simulation time 1.0000s. (Feed solution = CuSO_4 2%, spacer ML3- $\alpha 90^\circ \beta 0$, circled regions indicate the stagnant zones, $Re_f = 200$)	184
Figure 4.40	Contour plot of membrane wall shear stress and concentration in spacer filled membrane channel at simulation time 1.0000s. (Feed solution = CuSO_4 2%, spacer ML3- $\alpha 90^\circ \beta 0$, circled regions indicate the stagnant zones, $Re_f = 450$)	185

Figure 4.41	Area-averaged concentration polarization factor development for the membrane wall in the membrane channel filled with spacer ML3- α 120 β 30 between 0 -1s (a) Upper membrane wall (b) Lower membrane wall	186
Figure 4.42	Area-averaged concentration polarization factor development for the membrane wall in the membrane channel filled with spacer ML3- α 90 β 30 between 0 -1s (a) Upper membrane wall (b) Lower membrane wall	188
Figure 4.43	Design and optimization approach for spacer's design parameters	190
Figure 4.44	Supporting analysis to validate the optimum spacer design	193
Figure 4.45	Average Concentration factor (Γ) generated by different types of spacer filaments under specific range of λ (2000-50000)	194
Figure 4.46	Contour plot of velocity magnitude profile generated by different spacer filaments in membrane channel at Re_f 300 (a)Cylindrical filament (b) Rectangular filament (c) Hexagonal filament	196
Figure 4.47	Time-distance averaged wall shear stress, $\bar{\tau}$ generated by different types of spacer filaments under specific range of λ (2000-50000)	197
Figure 4.48	RMS of distance averaged wall shear stress fluctuation, $\bar{\tau}'_{RMS}$ generated by different types of spacer filaments under range of λ (2000-50000)	198
Figure 4.49	Concentration factor Γ generated by different spacer filaments at Re_f 300 (membrane located opposite to the spacers, data sampling at simulation time 1.0000s, vertical dotted lines indicate the location of the spacer)	200
Figure 4.50	Concentration factor Γ generated by different spacer filaments at Re_f 300 (membrane located adjacent to the spacers, data sampling at simulation time 1.0000s, vertical dotted lines indicate the location of the spacer)	200
Figure 4.51	Average concentration factor ($\bar{\Gamma}$) generated by spacers with different mesh length ratios under specific range of λ (2000-50000)	202

Figure 4.52	Effective concentration polarization factor, Ψ generated by spacer with different mesh length ratio (ML)	203
Figure 4.53	Contour plot of velocity profile magnitude generated by spacers with different mesh length ratio (ML) at Re_f 400 (a) ML2 (b) ML3 (c) ML4 (d) ML5 (e) ML6 (f) ML7	205
Figure 4.54	Time-distance averaged wall shear stress, $\bar{\tau}$ generated by spacer with different mesh length ratio (ML) under specific range of λ (2000-50000)	206
Figure 4.55	RMS of distance averaged wall shear stress fluctuation, $\bar{\tau}'_{RMS}$ generated by spacer with different mesh length ratio (ML) under specific range of λ (2000-50000)	207
Figure 4.56	Concentration factor Γ generated by spacer with different mesh length ratios at Re_f 400 (membrane located opposite to the spacers, data sampling at simulation time 1.0000s, vertical dotted lines indicate the location of the specific spacer) (a) Spacer ML2 – ML4 (b) Spacer ML5 - ML7	209
Figure 4.57	Concentration factor Γ generated by spacer with different mesh length ratios at Re_f 400 (membrane located adjacent to the spacers, data sampling at simulation time 1.0000s, vertical dotted lines indicate the location of the specific spacer) (a) Spacer ML2 – ML4 (b) Spacer ML5 - ML7	210
Figure 4.58	Average concentration factor ($\bar{\Gamma}$) generated by spacers with different mesh angle α and β under specific range of λ (2000-50000)	213
Figure 4.59	Effective concentration polarization factor, Ψ generated by spacers with different mesh angle α and β	214
Figure 4.60	Contour plot of wall shear stress (τ) profile and concentration factor (Γ) on membrane wall generated by spacer $\alpha 90\beta 0$ at Re_f 200	216
Figure 4.61	Contour plot of wall shear stress (τ) profile and concentration factor (Γ) on membrane wall generated by spacer $\alpha 90\beta 15$ at Re_f 200	216
Figure 4.62	Contour plot of wall shear stress (τ) profile and concentration factor (Γ) on membrane wall generated by spacer $\alpha 90\beta 30$ at Re_f 200	217

Figure 4.63	Contour plot of wall shear stress (τ) profile and concentration factor (Γ) on membrane wall generated by spacer $\alpha 90\beta 45$ at $Re_f 200$	217
Figure 4.64	Contour plot of wall shear stress (τ) profile and concentration factor (Γ) on membrane wall generated by spacer $\alpha 120\beta 80$ at $Re_f 200$	218
Figure 4.65	Contour plot of wall shear stress (τ) profile and concentration factor (Γ) on membrane wall generated by spacer $\alpha 120\beta 30$ at $Re_f 200$	219
Figure 4.66	Contour plot of wall shear stress (τ) profile and concentration factor (Γ) on membrane wall generated by spacer $\alpha 120\beta 60$ at $Re_f 200$	219
Figure 4.67	Contour plot of wall shear stress (τ) profile and concentration factor (Γ) on membrane wall generated by spacer $\alpha 30\beta 0$ at $Re_f 200$	220
Figure 4.68	Contour plot of wall shear stress (τ) profile and concentration factor (Γ) on membrane wall generated by spacer $\alpha 30\beta 15$ at $Re_f 200$	221
Figure 4.69	Time-area averaged wall shear stress, $\bar{\tau}$ generated by spacer with different mesh angle α and β under specific range of λ (2000-50000)	222
Figure 4.70	RMS of area averaged wall shear stress fluctuation, $\bar{\tau}'_{RMS}$ generated by spacer with different mesh angle α and β under specific range of λ (2000-50000)	222
Figure 4.71	Average concentration factor ($\bar{\Gamma}$) generated by spacers with different filament ratio (SFR) under specific range of λ (2000-50000)	225
Figure 4.72	Effective concentration polarization factor, Ψ generated by spacers with different filament ratio (SFR)	226
Figure 4.73	Contour plot of wall shear stress (τ) profile and concentration factor (Γ) on membrane wall generated by spacer U3L7 (3/7) at $Re_f 200$	227

Figure 4.74	Contour plot of wall shear stress (τ) profile and concentration factor (Γ) on membrane wall generated by spacer U4L6 (4/6) at Re_f 200	228
Figure 4.75	Contour plot of wall shear stress (τ) profile and concentration factor (Γ) on membrane wall generated by spacer U5L5 (5/5) at Re_f 200	228
Figure 4.76	Contour plot of wall shear stress (τ) profile and concentration factor (Γ) on membrane wall generated by spacer U6L4 (6/4) at Re_f 200	229
Figure 4.77	Contour plot of wall shear stress (τ) profile and concentration factor (Γ) on membrane wall generated by spacer U7L3 (7/3) at Re_f 200	229
Figure 4.78	Time-area averaged wall shear stress, $\bar{\tau}$ generated by spacer with different filament ratio (SFR) under specific range of λ (2000-50000)	231
Figure 4.79	RMS of area averaged wall shear stress fluctuation, $\bar{\tau}'_{RMS}$ generated by spacer with different filament ratio under specific range of λ (2000-50000)	231
Figure 4.80	Comparison of simulated and experimental channel pressure drop for optimum spacer filled membrane channels	234
Figure 4.81	Comparison of simulated and experimental permeation flux for optimum spacer filled membrane channels under different transmembrane pressure at Re_f 350. Notation: Δ = Experimental data, dotted line = simulation data	235

LIST OF PLATES

		Page
Plate 2.1	Commercial feed spacer	25
Plate 2.2	Anti-Telescoping Device (ATD)	25
Plate 2.3	Interconnector	26
Plate 2.4	Outer wrap for spiral wound membrane module (a) Typical glass wrapping process (b) Glass wrapping	26
Plate 3.1	Spacer fabrication frame (a) Side view of spacer fabrication frame (b) Plane view of spacer fabrication frame (c) Close view of spacer fabrication frame (d) Filament knots at spacer fabrication frame	124
Plate 3.2	Fabricated feed spacers (a) Spacer ML1.5- α 90 β 0 (b) Spacer ML3- α 90 β 0 (c) Spacer ML4.5- α 90 β 0 (d) Spacer ML6- α 90 β 0 (e) Spacer ML3- α 120 β 30 (f) Spacer ML3- α 120 β 0 (g) Spacer ML3- α 90 β 45 (h) Spacer ML3- α 90 β 30	125
Plate B.1	Photographic view of membrane permeation test cell	267
Plate B.2	Photographic view of experimental setup	268
Plate B.3	Photographic view of major equipment used in the experimental set-up	269

LIST OF SYMBOLS

A	computational face area (m ²)
c	equilibrium concentration of the solute in the solution (mmolL ⁻¹)
C	concentration (kg/m ³)
\bar{C}	average solute concentration across the membrane (kg/m ³)
C_g	gel concentration (kg/m ³)
d_f	Spacer diameter (m)
d_h	hydraulic diameter (m)
D_A	binary mass diffusion coefficient (m ² /s)
G	adsorbed quantity of organic (μgm ⁻²)
h	channel height (m)
h_{sp}	Spacer height (m)
J	mass flux (kg/s)
J_v	permeate flux (m/s)
J_{lim}	limiting flux (m/s)
k	mass transfer coefficient (m/s)
k_g	global mass transfer coefficient (m/s)
k_s	solute mass transfer coefficient (m/s)
\vec{L}	periodic length vector of the domain (m)
l	membrane channel length (m)
l_m	spacer mesh length (m)
L_p	hydraulic permeability (m/Pa.s)
M	molar mass of the adsorbing compound (g/mol)
ML	spacer mesh length ratio (dimensionless), defined by $ML = l_m/h$
m_A	solute mass fraction (kg solute/kg solution)
N_c	number of cell (dimensionless)
N_s	solute flux (kg/m ² ·s)
p	pressure (Pa)
$\overline{P_s}$	local solute permeability (m ² /s)
P_s	overall solute permeability (m/s)
\vec{r}	position vector (m)

R_o	observed rejection (dimensionless), defined by $R_o = (m_{A0} - m_{Ap}) / m_{A0}$
R_t	true rejection (dimensionless), defined by $R_t = (m_{Aw} - m_{Ap}) / m_{Aw}$
R_t'	$1 - R_t$ (dimensionless)
Re_f	feed Reynolds number (dimensionless), defined by $Re_f = \rho u_0 h / \mu$
Re_{ch}	channel Reynolds number (dimensionless), defined by $Re_{ch} = \rho u_0 d_h / \mu$
Re_p	permeation Reynolds number (dimensionless), defined by $Re_p = \rho J_v h / \mu$
Sc	Schmidt number (dimensionless), defined by $Sc = \mu / \rho D_A$
SFR	Spacer Filament Ratio (dimensionless), defined by $SFR = d_{f1} / d_{f2}$
Sh	Sherwood number (dimensionless)
S_{SP}	surface area of spacer (m^2)
St	Stanton number (dimensionless), defined by $St = k_g J_v$
S_{VSP}	specific surface of spacer (m^{-1})
t	time (s)
u	velocity in x-direction (m/s)
u_p	periodic velocity in x-direction (m/s)
v	velocity in y-direction (m/s)
v_p	periodic velocity in y-direction (m/s)
\vec{v}	velocity vector (m/s)
V	velocity magnitude (m/s)
\bar{V}	mean velocity magnitude, defined by $\bar{V} = \frac{1}{t} \times \int_0^t V(t) dx$
V'	fluctuation of velocity magnitude, defined by $V' = V - \bar{V}$
V'_{RMS}	Root Mean Square (RMS) of velocity magnitude fluctuation, defined by $V'_{RMS} = \sqrt{\frac{1}{t} \times \int_0^t V'^2(t) dt}$
V_{SP}	spacer volume (m^3)
V_{TOL}	Total volume (m^3)
w	velocity in z-direction (m/s)
w_p	periodic velocity in z-direction (m/s)
x	x coordinate (m)
y	y coordinate (m)
z	z coordinate (m)

Greek letters

α	angle between the upper and lower spacer filaments (°)
β	angle between the spacer and the mean flow direction (°)
$\beta(\bar{r})$	linearly-varying component of the pressure (Pa)
Γ	concentration factor (concentration polarization factor) (dimensionless), defined by $\Gamma = (C_{AW}/C_{A0}) - 1$
$\bar{\Gamma}$	average concentration polarization factor (dimensionless), defined by $\bar{\Gamma} = \frac{1}{L} \times \int_0^L \Gamma(x) dx$ or $\bar{\Gamma} = \frac{1}{A} \times \int_{A1}^{A2} \Gamma(A) dA$
λ	Specific power consumption (Pa/s), defined by $\lambda = \Delta p u / l$
ε	porosity (dimensionless)
σ	reflection coefficient (dimensionless)
δ	boundary layer thickness (m)
δ_c	distance between membrane wall and adjacent cell centroid value (m)
π	osmotic pressure (Pa)
ρ	density (kg/m ³)
τ	instantaneous wall shear stress (Pa)
$\bar{\tau}$	distance averaged wall shear stress (Pa), defined by $\bar{\tau} = \frac{1}{l} \times \int_{l1}^{l2} \tau(l) dl$ or area averaged wall shear stress (Pa), defined by $\bar{\tau} = \frac{1}{A} \times \int_{A1}^{A2} \tau(A) dA$
$\bar{\bar{\tau}}$	time-distance (area) averaged wall shear stress (Pa), defined by $\bar{\bar{\tau}} = (\text{Pa}) \frac{1}{t} \times \int_0^t \bar{\tau}(t) dt$
$\bar{\tau}'$	distance averaged wall shear stress fluctuation (Pa), defined by $\bar{\tau}' = \bar{\tau} - \bar{\bar{\tau}}$
$\bar{\tau}'_{RMS}$	Root Mean Square (RMS) of distance averaged wall shear stress fluctuation (Pa), defined by $\bar{\tau}'_{RMS} = \sqrt{\frac{1}{t} \times \int_0^t (\bar{\tau}')^2(t) dt}$
$\bar{\bar{\tau}}_e$	effective time-distance (area) averaged wall shear stress (Pa), defined by $\bar{\bar{\tau}}_e = \frac{1}{\Delta \lambda} \int_{\lambda1}^{\lambda2} \tau(\lambda) d\lambda$

$\bar{\tau}'_{e\prime RMS}$	effective RMS of distance (area) averaged wall shear stress fluctuation (Pa), defined by $\bar{\tau}'_{e\prime RMS} = \frac{1}{\Delta\lambda} \int_{\lambda_1}^{\lambda_2} \bar{\tau}'_{RMS}(\lambda) d\lambda$
\bar{t}	stress tensor (Pa)
Ψ	effective concentration polarization factor, defined by $\frac{1}{\Delta\lambda} \int_{\lambda_1}^{\lambda_2} \bar{\Gamma}(\lambda) d\lambda$
μ	viscosity (kg/m.s)
ΔP	transmembrane pressure (Pa)
Δp_{ch}	cross channel pressure drop (Pa/m)
ω	solute permeability (kg/(N.s))
α_p	under-relaxation factor for pressure (dimensionless)
ϕ	computational cell center value
ϕ_k	user defined scalar
φ	inclination angle (°)
Γ_k	diffusion coefficient for user defined scalar
$\Delta \vec{s}$	displacement vector from the upstream cell centroid to the face centroid (m)
$\nabla \tilde{p}(\vec{r})$	periodic pressure (Pa)

Subscripts

0	feed solution
b	bulk/feed solution
BL	boundary layer
c	centroid value of the cell adjacent to the membrane wall
f	face value
im	imbalance mass
in	inlet
nb	in the cell
p	permeate side
s	solute
w	solution adjacent to the wall

LIST OF ABBREVIATIONS

AMG	Algebraic Multigrid method
ATD	Anti Telescoping Device
BC	Boundary condition
CFD	Computational Fluid Dynamics
CP	Concentration Polarization
DOTM	Direct Observation Through the Membrane
DS	Direct Simulation
DSPM	Donnan Steric Pore Flow Model
ENP	Extended Nernst-Planck
FDM	Finite Difference Method
FEM	Finite Element Method
FG	spacer filament geometry
FVM	Finite Volume Method
ID	Inner diameter
ML	spacer mesh length ratio
MPPIS	Multiple Cells Permeation Properties Integrated Simulation
NF	Nanofiltration
OD	Outer diameter
PUCS	Periodic Unit Cell Simulation
PPIS	Permeation Properties Integrated Simulation
RO	Reverse Osmosis
RMS	Root Mean Square
SK	Speigler-Kedem
SIMPLE	Semi-Implicit Method for Pressure-Linked Equations
SPPIS	Single Cell Permeation Properties Integrated Simulation
SWM	Spiral Wound Membrane
UDF	User Defined Function
UDS	User Defined Scalar
UF	Ultrafiltration
2-D	2 Dimensional
3-D	3 Dimensional

PERUANG SUAPAN MODUL MEMBRAN “SPIRAL WOUND” UNTUK PENURASAN NANO DAN OSMOSIS BALIKAN: PEMODELAN, SIMULASI DAN REKABENTUK

ABSTRAK

Sejak 1970an, permintaan untuk modul membran “spiral wound” (SWM) meningkat dengan mendadak di kedua-dua pasaran tempatan dan antarabangsa. SWM yang terdapat di pasaran mempunyai jangka penggunaan di antara satu hingga tiga tahun bergantung kepada aplikasi masing-masing. Untuk memanjangkan jangka penggunaan SWM, faktor yang paling utama adalah rekebetuk peruang suapan SWM yang optimum untuk mengatasi masalah kotoran. Disebabkan masalah kotoran di SWM bermula dengan pembentukan pengutuban kepekatan dan peruang suapan yang berbeza akan menjana tahap kehilangan tenaga yang berlainan, satu peruang suapan yang optimum telah direkabentuk berdasarkan pengutuban kepekatan dan kehilangan tenaga dengan menggunakan kaedah Pengkomputeran Bendalir Dinamik (CFD).

Dengan integrasi sifat-sifat penelapan, kod CFD komersial Fluent 6 telah digunakan untuk simulasi hidrodinamik di dalam saluran suapan SWM yang kosong. Model CFD tersebut telah disahkan secara eksperimen dari segi sifat-sifat penelapan. Berdasarkan keputusan kajian, ia membuktikan membran perlu dimodelkan sebagai dinding telap dengan fluks telapan berubah. Selain itu, kesan suapan nombor “Reynolds” (Re_f), tekanan antara membran dan zat terlarut ke atas perkembangan pengutuban kepekatan telah dikaji. Untuk simulasi saluran suapan SWM yang berisi peruang, sifat-sifat penelapan telah berjaya diintegrasikan ke dalam penyelesaian persamaan-persamaan menakluk dan disahkan secara eksperimen.

Berdasarkan analisa hidrodinamik tidak mantap, pembentukan hidrodinamik tidak mantap di saluran suapan SWM yang berisi peruang boleh dikesan pada nombor “Reynolds” yang rendah (Re_f 100-300) pada jarak peralihan tertentu dari lokasi saluran

masuk. Rekebentuk peruang yang berbeza didapati menghasilkan tahap hidrodinamik tidak mantap yang berlainan. Dalam kajian ini, kehilangan tenaga di saluran suapan SWM yang berisi peruang telah ditentukan dengan menggunakan kuasa penggunaan tentu (λ). Rekebentuk peruang yang berbeza didapati menjana tahap λ yang berlainan. Berdasarkan keputusan eksperimen dan simulasi, hidrodinamik tidak mantap di saluran suapan SWM yang berisi peruang boleh mengganggu pembentukan pengutuban kepekatan.

Parameter rekebentuk untuk peruang suapan yang terdiri daripada geometri filamen peruang (FG), nisbah jarak jejaring (ML), sudut jejaring (α and β) dan nisbah filamen telah dioptimumkan berdasarkan faktor pengutuban kepekatan berkesan (Ψ) yang minimum, di mana seterusnya disahkan dengan analisa tegasan ricih dinding, profil plot kontor dan pengutuban kepekatan setempat. Berdasarkan keputusan kajian, filamen silinder yang sama saiz dengan nisbah jarak jejaring 3 dan sudut jejaring ($\alpha=120^\circ$ and $\beta=30^\circ$) merupakan parameter rekebentuk peruang yang optimum.

Model optimum peruang tersebut telah disahkan secara eksperimen dari segi hidrodinamik dan sifat-sifat penelapan. Berdasarkan perbandingan prestasi secara eksperimen dengan peruang yang lain, peruang optimum menjana fluks peningkatan yang tertinggi dan melebihi 100% berbanding dengan saluran membran kosong. Peruang optimum juga menjana peningkatan fluks (lebih kurang 6%-11%) lebih tinggi berbanding dengan peruang yang lain dengan nisbah jarak jejaring (ML=3) dan sudut jejaring ($\alpha=120^\circ$ dan $\beta=30^\circ$) yang sama. Berdasarkan perbandingan penyingkiran cerapan, peruang optimum menghasilkan penyingkiran cerapan yang tertinggi berbanding dengan peruang yang lain dengan nisbah jarak jejaring dan sudut jejaring yang sama.

FEED SPACER OF SPIRAL WOUND MEMBRANE MODULE FOR NANOFILTRATION AND REVERSE OSMOSIS: MODELING, SIMULATION AND DESIGN

ABSTRACT

Since 1970s, the demand for spiral wound membrane (SWM) has been rapidly increasing in both local and worldwide market. Current market available SWM possess lifespan between one to three years depends on the applications. In order to extend SWM lifespan, the most influencing factor is the design of optimal SWM feed spacer to overcome fouling problem. Since fouling problem in SWM starts with the formation of concentration polarization and different feed spacers generates different degree of energy loss, an optimal feed spacer was designed based on the concentration polarization and energy loss using Computational Fluid Dynamics (CFD) approach.

With the integration of permeation properties, commercial CFD code Fluent 6 was employed to simulate the hydrodynamics in the empty SWM feed channel. The integrated CFD model was validated experimentally in terms of permeation properties. Based on the results of the study, it proved that the membrane interface should be modeled as permeable wall with varying permeate flux. Besides that, the effect of feed Reynolds number, transmembrane pressure and solutes on concentration polarization development was studied. In the spacer filled SWM feed channel simulation, permeation properties were successfully incorporated in the solution of governing equations and validated experimentally.

Based on the unsteady hydrodynamics analysis, the emergence of unsteady hydrodynamics in the spacer filled SWM feed channel can be detected at low feed Reynolds number (Re_f 100-300) at certain transition length from the channel entrance. Different spacer designs were found to produce different magnitude of unsteady hydrodynamics. Under current study, energy loss in the spacer filled SWM feed

channel was determined using specific power consumption (λ). Different spacer designs were found to generate different degree of λ . Based on the experimental and simulated results, the unsteady hydrodynamics in the spacer filled SWM feed channel can significantly disrupt the development of concentration polarization.

Feed spacer design parameters which consisted of spacer filament geometry (FG), mesh length ratio (ML), mesh angles (α and β) and filament ratio (SFR) were optimized based on the minimum effective concentration polarization factor, Ψ which further validated by wall shear stress analysis, contour plot profile and localized concentration factor. Based on current study, equal cylindrical filaments with mesh length ratio 3 and mesh angle ($\alpha= 120^\circ$ and $\beta=30^\circ$) was the optimum spacer design parameters.

The optimum spacer model was validated experimentally in term of hydrodynamics and permeation properties. Based on the experimental performance comparison with others spacers, optimum spacer generated the highest flux enhancement which was more than 100% as compared to empty membrane channel. Optimum spacer generated higher flux enhancement (approximately 6%-11%) as compared to spacers with identical mesh length ratio (ML=3) and mesh angles ($\alpha=120^\circ$ and $\beta=30^\circ$). Based on the observed rejection comparison, optimum spacer yielded the highest observed rejection as compared to the spacers with identical mesh length ratio or mesh angles.

CHAPTER 1

INTRODUCTION

1.1 Membrane processes

A membrane is a permeable or semi-permeable phase, often a thin polymeric solid, which restricts the motion of certain species. This membrane or barrier controls the relative rates of transport of various species through itself and thus, as with all separations, gives one product depleted in certain components and second product concentrated in these components. The membrane processes can be categorized based on its separation mechanism which mainly consist of size exclusion, solubility and diffusivity and charge (van Rijn, 2004). Table 1.1 shows the major membrane processes arranged according to the mechanism of separation. Membrane separation processes that occur based on size exclusion involve microfiltration, ultrafiltration and nanofiltration. Microfiltration membrane consists of the largest membrane pores (which typical range from 0.1 -10 μm) as compared to the nanofiltration and ultrafiltration membrane. These types of membranes commonly applied in prefiltration in water treatment, sterile filtration, beverage clarification, screening of bacteria and etc.

Table 1.1: Membrane processes arranged according to the mechanism of separation (van Rijn, 2004)

Separation Mechanism	Major membrane separation process
Size exclusion (filtration)	Nanofiltration, ultrafiltration, microfiltration
Solubility/ diffusivity	Reverse osmosis, gas separation, pervaporation
Charge	Electrodialysis

Ultrafiltration mainly used to remove particles in the size range 0.001-0.1 μm . Solvents and salts of low molecular weight will pass through the membranes whilst larger molecules are retained. Generally, ultrafiltration membrane is classified by molecular weight cut-off and by notional pore size. These type of membrane commonly used in separation of macromolecular solutes and colloidal material from

macromolecular solutes and solvents. The applications of these membranes include concentration of protein/enzyme for pharmaceutical and biomedical industries, food and dairy, pulp and paper and etc (Scott and Hughes, 1996).

Nanofiltration is a relatively young description for filtration processes using membrane with a pore ranging 0.5 to 1nm. In general, nanofiltration is used to separate relatively small organic compound and (multivalent) ions from a solvent. Nanofiltration systems typically operate at lower pressure than reverse osmosis but yield higher flowrates of water with a different quality to reverse osmosis. The application areas for nanofiltration cover purification of sugar from acids, salts from dyes, water treatment, electroplating and etc (Baker, 2000).

In order to facilitate the separation process on molecular scale, a relatively dense membrane is required. The transportation mechanism of solute through this denser membrane is controlled by solution-diffusion process instead of size exclusion. This process involves dissolve and transportation, diffusion of solvent in the membrane through the membrane with driving force acting inside the membrane. The driving force is solely activated by properties of the membrane material like chemical affinity instead of porosity of the membrane. Major membrane processes that exhibit solution-diffusion mechanism include reverse osmosis, gas separation and pervaporation.

Reverse osmosis membranes can essentially separate all solutes species, both inorganic and organic from the solution. The particle size range for the applications of reverse osmosis is approximately 0.2 – 0.5nm. Reverse osmosis has been widely applied in aqueous solution processing like desalination of brackish and seawater, production of ultra pure water for semiconductor, concentration of solutions of food products, pharmaceutical solutions and chemical streams, wastewater treatment and etc (Baker *et al.*, 1991).

Gas separation processes mainly conducted using gas permeation membrane (non-porous membrane) which essentially depends on the differences in permeability and diffusivity of the gaseous components. The solubility of gaseous component in the membrane will combine with diffusion to determine the permeability and selectivity of separation. Gas permeation membranes find their major applications in chemical and petrochemical industries like separation and recovery of hydrogen from refinery gas and purification of natural gas. Other applications include the separation of oxygen and nitrogen from air, dehydration of gases, methane recovery from biogas and etc (Nunes and Peinemann, 2001).

Third type of membrane process that exhibits solution-diffusion mechanism is pervaporation. This process essentially applied in separation of liquid-liquid mixture with an azeotropic composition with relatively small difference in volatility. Applications that use this process include dehydration of ethanol, acetic acid, removal of ethanol for fermentation products and etc.

During separation process, the charge of a molecule may affect its transport properties through a medium, or a charged molecule may selectively be exchanged for another charged molecule. The incorporation of ion-exchange groups in the membrane material produces a semi-permeable barrier that allows passage of either positively charged ions or negatively charged ions while excluding passage of ions of the opposite charge. These semi-permeable barriers are commonly known as electrodialysis membranes. The major applications for electrodialysis are in desalting and concentrating seawater in salt production, concentration or dilution of electrolyte solutions in desalination of brackish water, effluent treatment for salt solution in food, pharmaceutical and electroplating industry and etc (van Rijn, 2004).

1.2 Membrane module

The feasibility of a membrane process depends on the design of membrane module since the active separation membrane area is directly influenced by the membrane module configuration. The cost reduction of membrane module has led to the commercialization of membrane process in the 1960s and 1970s (Baker *et al.*, 1991). Plate-and-frame and tubular membrane module are two of the earliest module design that based on simple filtration technology. Both systems are still available until today, but due to their relatively high cost and inefficiency, they have been mainly substituted by hollow fiber and spiral wound membrane.

1.2.1 Plate-and-frame module

Plate-and-frame modules were among the earliest types of membrane systems and the design is principally based on conventional filter press. Membrane feed spacers and product spacers are layered together between two end plates, as shown in Figure 1.1. The comparatively high production cost (as compared to others membrane modules) and leaks caused by the numerous gasket seals in the system has restricted the usage of this system to small scale application. The use of plate-and-frame is now generally limited to electro dialysis and pervaporation systems (Baker *et al.*, 1991).

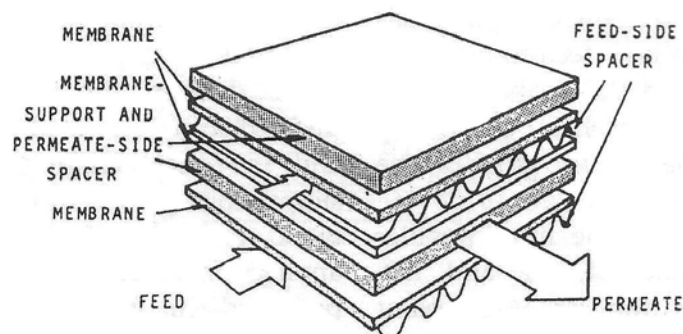


Figure 1.1: Plate-and-frame membrane module (Baker *et al.*, 1991)

1.2.2 Tubular module

Polymeric tubular membranes are usually made by casting a membrane onto the inside of a pre-formed tube, which is referred to as the substrate tube (Figure 1.2). These are mainly made from non-woven fabrics such as polyester or polypropylene. The diameter of tubes range from 5-25mm, with 12.5mm in common usage. There are mainly two types of housing system for tubular membrane module which known to be the supported and unsupported tubes housing system. Basically, in supported housing system, membrane tube is supported by perforated or porous stainless steel tubes. A bundle of these membrane tubes is mounted into a vessel that collect permeation and caps are fitted to the end to give different flow pattern. Exhibiting high mechanical strength, this type of module can be used at high pressure (up to 60 bar) separation process like reverse osmosis. In the unsupported housing design, the membrane is supported only by substrate tube and a cartridge is constructed by potting the ends of a bundle of tubes in an epoxy resin. These types of designs offer lower capital cost than the supported tube module but, it has a reduced tolerance to pH, pressure and temperature (Baker *et al.*, 1991).

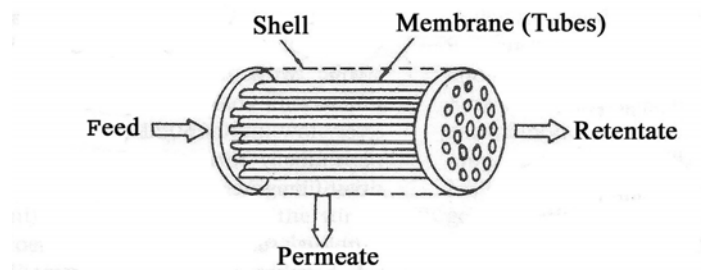


Figure 1.2: Tubular membrane module (Baker *et al.*, 1991)

1.2.3 Hollow fiber module

There are two basic configurations for hollow-fiber membrane module. The first is the closed-end design as shown in Figure 1.3. In this module, a loop of fiber or a closed bundle is contained in a pressure vessel. The system is pressurized from the shell side and permeate passes through the fiber wall and exits via the open fiber ends.

This design allows large fiber membrane areas to be contained in an economical system. Since the fiber wall supports a considerable hydrostatic pressure, these fibers usually have a small diameter, around 100μ ID and $\sim 200\mu\text{m}$ OD (Baker *et al.*, 1991). The second basic design for hollow fiber module is more common (Figure 1.4). In this case, the fibers are laid out parallel to each other in bundles and the open ends are then cast into two resin blocks which are bonded into shrouds to form a cartridge. In order to minimize the pressure drops in the inside of the fibers, the fibers often have larger diameters than fine fibers used in closed loop system. Membrane in these configurations are available for reverse osmosis, ultrafiltration and microfiltration applications such as seawater desalination, water clarification, fruit clarification, eletrophoretic paint recovery, oil waste water treatment and etc (Scott *et al.*, 1996).

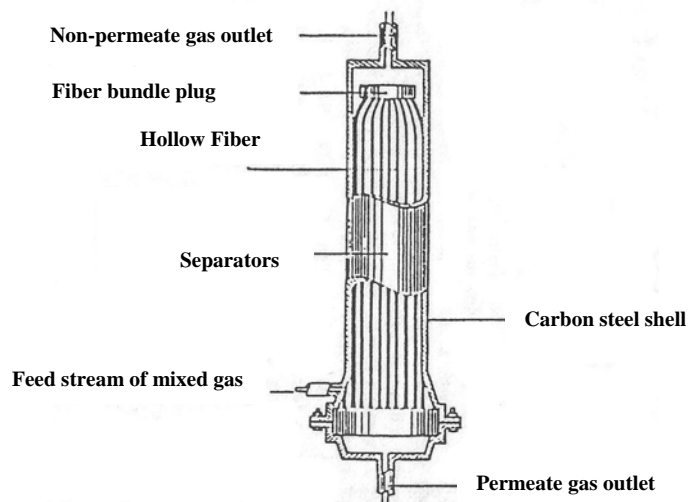


Figure 1.3: Hollow fiber module with closed-end design (Scott *et al.*, 1996)

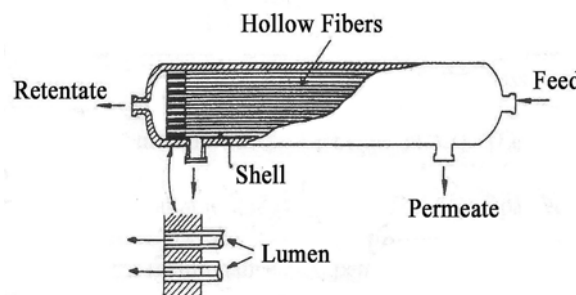


Figure 1.4: Hollow fiber module with opened-end design (Scott *et al.*, 1996)

1.2.4 Spiral wound module

The designs of a spiral wound membrane consist of membrane envelopes (leaves) and feed spacers which wound around a perforated central collection tube. A schematic diagram of an open spiral wound membrane is shown in Figure 1.5. Based on the figure, feed solution passes axially down the module across the membrane envelope. A portion of the feed solution permeates into the membrane envelope, where it spirals toward the center and exits through the collection tube (Scott *et al.*, 1996).

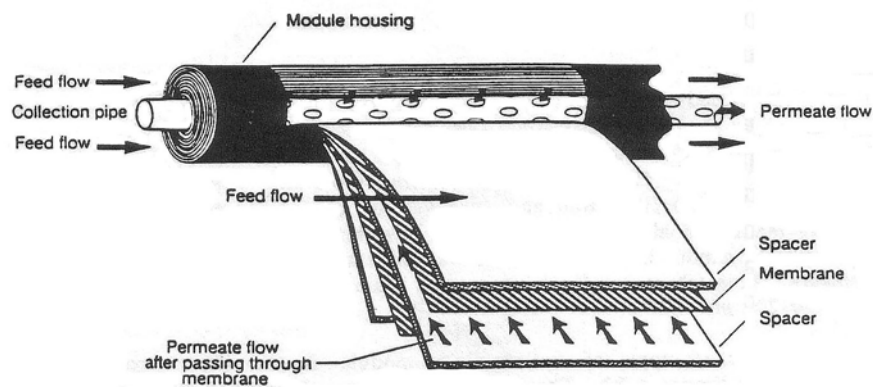


Figure 1.5: Spiral Wound Membrane Module (Scott *et al.*, 1996)

These modules were designed in an effort to pack as much membrane surface as possible into a given volume (Senthilmurugan *et al.*, 2005). Small scale spiral-wound modules consist of a single membrane leaf wrapped around the collection tube. In the large membrane area module, using single membrane leaf might generate large pressure drop due to the longer path taken by the permeate to reach the central collection tube. Multiple short leaves have been utilized to keep the pressure in the module in a manageable level (Van der Meer and van Dijk, 1997).

1.3 Membrane module market demand

Since 1960s, the search for viable alternatives to traditional energy-intensive separation methods such as distillation, has led to the introduction of processes based on membranes. Membrane technology often offers cheaper capital and utility costs and has displaced conventional separation techniques in many areas (Avlonitis *et al.*, 1995; Nunes and Peinemann, 2001). The demand for more efficient and reliable membranes is directing research towards producing new membranes with higher water flux, better salt rejection properties and better resistance to chemical attack (Baker, 2000). The rapid expansion is to be ascribed to the simplicity, economy and improved reliability of present industrial installation. This in turn is due to both better membrane performance and improved module design (Scott and Hughes, 1996; van Rijn, 2004).

Based on a recent business survey, the market for cross-flow membrane modules and equipment to purify water and other liquids will grow from USD7.6 billion in 2006 and predicted to excess USD10 billion in 2010. The annual growth rate for membrane markets is estimated at around 10-15% (Filtration Industry Analyst, 2006). The cross-flow membrane modules market is divided into three major segments. The largest is reverse osmosis (RO) accounting for 50% of the total sales. Most of the reverse osmosis membranes are manufactured in spiral wound membrane module and hollow fiber membrane module. This is the most efficient membrane and is used for desalination, creation of ultrapure water for electronics and pharmaceutical applications. The other 50% of the market is almost evenly split between ultrafiltration and microfiltration. Besides, in 2009, it is predicted that the leading segment for cross-flow membranes will be desalination with sales of equipment and membranes in excess of \$2.2 billion worldwide (Membrane Technology, 2006) as shown in Figure 1.6. Besides, the price of spiral-wound modules has decreased almost 50% in the past decade (Semiat, 2001) and new energy recovery devices with efficiencies as high as 98% have been introduced in the desalination industries for the last few years (Drablos,

2001; Geisler *et al.*, 2001). With cheaper capital cost and improved efficiencies, spiral wound membrane has been used intensively in the desalination industries and is predicted to dominate the desalination industries in the near future (Semiati, 2001).

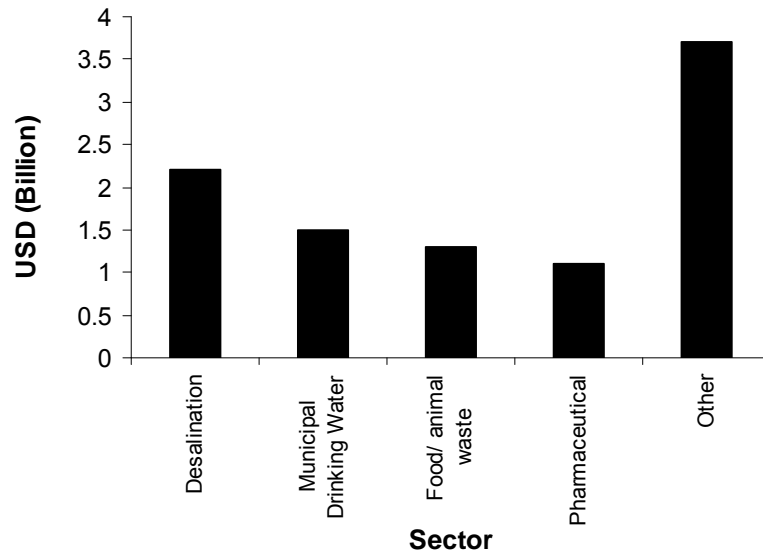


Figure 1.6: World membrane market at 2009 (Membrane Technology, 2006)

The Asian membrane market will grow at a faster rate than other regions due to the lack of clean water and the rapid growth of the electronics and pharmaceutical industries. As the leading export sector in Malaysia, electrical and electronic products made up 52.9% of total Malaysian Exports in 2003 (Aseansources, 2006). The biggest export item is semiconductor devices used in a diverse range of industries, such as automotive and telecommunications. The growth of semiconductor industries has promoted a high demand for ultrapure water, which subsequently contributes to the growth of local membrane market. Spiral wound membrane has been widely used in the semiconductors industries to produce ultrapure water for wafer rinsing process.

At present, the demand for spiral wound membrane is considerable high in both local and worldwide market. In the near future, it is also being forecasted to the most demanding membrane module. The extensive usage of spiral wound membrane is contributed by its added features in term of configurations and designs.

1.4 Advantages in spiral wound membrane

In reverse osmosis, nanofiltration and ultrafiltration, most membrane modules are fabricated in hollow fiber or spiral wound design. High packing density and low manufacturing cost are the major factors that contribute to the extensive usage of these membrane modules in various industries (refer to Table 1.2). Plate-and-frame and tubular modules solely used in a few applications where membrane fouling is particularly severe, for example, food applications or processing of heavily contaminated industrial water (Chaabane *et al.*, 2006).

Fouling resistance is one of the major factors to determine the module selection (Schwinge *et al.*, 2002). Generally, membrane fouling is a critical problem in liquid separations such as reverse osmosis, nanofiltration and ultrafiltration. Although plate-and-frame and tubular modules have better fouling control ability, these types of modules are not preferable due to high selling price except for severe fouling separation process. Comparing between the hollow fiber and spiral wound modules, spiral wound modules appear to be displacing hollow fiber design because they have more fouling resistance which apparently reduces the cost for the feed pretreatment (Pavlova *et al.*, 2005).

Table 1.2: Characteristics of major membrane module designs (Baker *et al.*, 1991)

	Hollow Fibers	Spiral Wound	Plate-and-Frame	Tubular
Manufacturing cost (\$USD/m ²)	5-20	30-100	100-300	50-200
Packing density	high	moderate	low	low
Resistance to fouling	very poor	moderate	good	very good
Parasitic pressure drops	high	moderate	moderate	low
Suitability for high pressure operation	yes	yes	can be done with difficulty	can be done with difficulty
Limitation to specific types of membranes	yes	no	no	no

Besides, the fabrication of spiral wound membrane also has less limitation to specific types of membranes as compared to the hollow fiber membrane. This added feature principally allows more types of membrane to be fabricated in spiral wound design. Enhanced stability under high pressure and moderate parasitic pressure drops in spiral wound membrane has also promoted the wide-ranging usage of this module in various sectors (Roth *et al.*, 2000; Champlin *et al.* 2000; Al Wazzan *et al.*, 2002; Bergen *et al.*, 2004).

1.5 Problem statement

Membrane fouling is a critical problem in liquid separations such as reverse osmosis, nanofiltration and ultrafiltration. The occurrence of these phenomenon constraints the normal membrane separation process and reduce the lifespan of the spiral wound membrane module. The fouling problem in spiral wound membrane basically starts with the formation concentration polarization phenomenon. Concentration polarization is normally formed rapidly at the beginning of filtration and causes a reduction in flux predominantly due to the increased osmotic pressure of retained ions and the formation of gels by retained organic molecules. Colloidal deposits can further increase concentration polarization by forming an unstirred layer that increases the boundary layer concentration. The intensive development of concentration polarization at the membrane surface will contribute to more problematic fouling mechanism such as gel polarization, adsorption and scaling of solute.

Although spiral wound membranes have better fouling resistance as compared to hollow fiber membrane, yet due to their unique design and construction, the fouling control methods for spiral wound membranes are limited to hydrodynamics, pretreatment and operational method as demonstrated in Table 1.3. Chemical cleaning and backflushing are inappropriate for spiral wound membranes since the

tightly wrapped structures are not easily to be opened for cleaning or to be operated in reverse direction. Pretreatment and operational method can control the fouling problem in spiral wound membranes, but these methods principally increase the overall operating cost for the separation processes with spiral wound membranes. Moreover, to overcome the fouling problem due to concentration polarization, these methods are inappropriate to be employed in the spiral wound membrane.

Table 1.3: Foulants and their control strategies in spiral wound membrane module for nanofiltration and reverse osmosis processes (Schafer *et al.*, 2005)

Foulant	Fouling control
General/ Concentration Polarization	Hydrodynamics/ shear (novel spacer design or higher cross flow velocity)
Inorganic (Scaling)	Operate below solubility limit, pretreatment, reduce pH 4-6 (acid addition), low recovery, anti-scalants
Organics	Pretreatment using biological processes, activated carbon, ion exchange, ozone, enhanced coagulation.
Biological solids	Pretreatment using disinfection (i.e. chlorination), filtration, coagulation, microfiltration, ultrafiltration.

Alternatively, concentration polarization and fouling problem can be effectively controlled by varying the hydrodynamics conditions in the spiral wound membrane channel. This can be achieved by the introduction of higher cross flow velocity or by the incorporation of an optimized feed spacer in the membrane channel. The increment of operational cross flow velocity can directly produce higher scouring force and reduces the development of concentration polarization and fouling on the membrane surface. The drawback of using this method is the requirement of higher pumping energy to facilitate the energy loss generated across the spacer-filled feed channel. In order to suppress concentration polarization and fouling problem with moderate energy loss, optimized feed spacer is needed in the spiral wound membrane feed channel. An optimized feed spacer is capable to generate unsteady hydrodynamics in the membrane channel, which subsequently reduce the occurrence potential of concentration polarization and fouling at minimum level of energy loss.

In order to design and optimize the feed spacer, detail understanding on the hydrodynamics and permeation properties in spacer-filled spiral wound feed channel is crucial to balance the trade-off between concentration polarization reduction and energy loss generation. The flow and permeation properties should be modeled or simulated locally with the consideration of actual hydrodynamics. Computational Fluid Dynamics (CFD) simulation and modeling approach have been conducted to predict hydrodynamics in the spacer filled membrane channel parallel with the development of special numerical CFD codes and CFD simulation software (Rosen and Tragardh, 1993; Ghidossi *et al.*, 2006). This method potentially offers faster approach to determine the optimum feed spacer design parameters if compared with experimental methods. This attempt had also been supported by the improvement of the computational power which offers potential solution for millions of numerical grids. Spacer designs conducted by CFD can be subdivided into two categories which are CFD simulation and CFD mathematical modeling.

Generally, CFD simulation approaches are conducted using commercial CFD simulation code. The improvements in CFD simulation technique and methodology had accelerated the simulations speed and offer the visualization of fluid's flow pattern in the complex 3-D spacer-filled SWM feed channel domain. However, CFD simulations for fluid's flow in the membrane channel are found to be restricted to hydrodynamics conditions whereby the membrane interface is treated as an impermeable wall. Due to this limitation, permeation properties such as permeation flux and true rejection were neglected in the design and optimization of the feed spacers (Karode and Kumar, 2001; Li *et al.*, 2002b; Schwinge *et al.*, 2003; Ranade and Kumar 2006b). These assumptions have neglected the mass transport across the membrane and might lead to the incorrect assessment of the concentration polarization phenomenon.

In order to give a better description for concentration polarization, CFD mathematical modeling have been applied as a rigorous tool to model concentration polarization through the solution of the continuity, Navier–Stokes and solute continuity equations (Geraldes *et al.*, 1998; Geraldes *et al.*, 2000; Geraldes *et al.*, 2001; Ma *et al.* 2004; Ma *et al.*, 2005). Permeation properties such as permeation flux and true rejection were incorporated in the membrane boundary condition. Since CFD mathematical modeling employed special numerical code, this method was technically restricted to empty or simple 2D spacer filled membrane channel. Thus, CFD mathematical modeling was insufficient to model the actual hydrodynamics and concentration polarization in the spiral wound membrane feed channel.

Thus, a CFD simulation approach (which uses commercial CFD codes) which integrated with permeation properties is needed to model and simulate the actual hydrodynamics and permeation properties in the spiral wound membrane feed channel for designing and optimizing the feed spacer based on concentration polarization and energy loss. The comparisons of different CFD approaches to model and simulate the SWM feed channel are listed in Table 1.4.

Table 1.4: Comparison of different CFD approaches to model SWM feed channel

CFD Approaches	Advantages	Limitations
CFD Simulation	Simulate and visualize the hydrodynamics for the complex 2D and 3D spacer filled membrane channel.	Permeation properties are neglected. Membrane is treated as non-permeable wall.
CFD Mathematical Modeling	Model the hydrodynamics and permeation properties in the membrane channel.	Limited to empty or simple 2D spacer filled membrane channel.
CFD Simulation integrated with permeation properties	Simulate and visualize the hydrodynamics and permeation properties for the complex 2D and 3D spacer filled membrane channel.	No limitation.

1.6 Project objectives

The objectives of this project are subdivided into the main objective and the measurable objectives.

1.6.1 Main objective

To design and optimize feed spacer of spiral wound membrane (SWM) module based on concentration polarization and energy loss using integrated Computational Fluid Dynamics (CFD) simulation approach for nanofiltration and reverse osmosis process.

1.6.2 Measurable objectives

To achieve the main objective, the measurable objectives for current study consist of:

- To incorporate permeation properties in the empty SWM feed channel simulation and validate this integrated CFD model experimentally.
 - To validate the permeation properties for the empty SWM channel.
 - To study the effect of feed Reynolds number, transmembrane pressure and solutes on the concentration polarization development.

- To incorporate permeation properties in the spacer filled SWM feed channel simulation and validate this integrated CFD model experimentally.
 - To validate the hydrodynamics properties for the spacer filled SWM channel.
 - To validate the permeation properties for the spacer filled SWM channel.

- To study the unsteady hydrodynamics and energy loss in the spacer filled SWM feed channel.
 - To study the effect of spacer design parameters on unsteady hydrodynamics.
 - To study the effect of spacer design parameters on energy loss.
 - To study the effect of unsteady hydrodynamics on concentration polarization.

- To optimize the feed spacer design parameters in terms of concentration polarization factor and energy loss based on the following design parameters:
 - Spacer filament geometry
 - Spacer mesh length ratio
 - Spacer mesh angles
 - Spacer filament ratio

- To validate the optimum feed spacer's designs experimentally and compare the performance of the optimized spacer with other feed spacers.
 - To validate the hydrodynamics properties for the optimum spacer filled membrane channel.
 - To validate the permeation properties for the optimum spacer filled membrane channel.
 - To conduct performance comparison between optimum spacer and other spacers based on permeation flux and observed rejection.

1.7 Scope of research project

Current study employed commercial CFD code Fluent 6 for simulating the hydrodynamics in the empty membrane channel to design and optimize the feed spacer. In order to estimate the concentration polarization accurately, permeation properties which consisted of permeation flux and membrane wall concentration were integrated as the membrane boundary conditions in the solution of the governing equations (mass conservation equation, Navier-Stokes equations and solute conservation equation). These permeation properties were written in "C" language and incorporated in the commercial CFD simulator as User Defined Function (UDF). This integrated CFD model for empty membrane channel was validated experimentally in terms of permeation properties. Effects of feed Reynolds number, transmembrane

pressure and solutes on the development of concentration polarization were studied for empty SWM channel.

Using similar approach, permeation properties were incorporated in the spacer filled SWM channel simulation. In order to confirm the validity of the integrated CFD model for the spacer filled membrane channel, the simulated hydrodynamics and permeation properties were further verified by experimental data. Under the simulated hydrodynamics validation, simulated channel pressure drop data were compared with the experimental results. Under the permeation properties validation, simulated permeation fluxes were compared with the experimental permeation fluxes.

Generally, the typical operational feed Reynolds number for spiral wound membrane ranges from 50 to 500 (Li *et al.*, 2002b). Since the hydrodynamics in the confined space of feed spacer can achieve unsteady state within this range of feed Reynolds number, it is appropriate to employ unsteady simulation to investigate the unsteady hydrodynamics and its influence on concentration polarization alleviation in the spiral wound membrane feed channel. The unsteady hydrodynamics analysis included the effects of entrance transition length, spacer filament geometries, mesh length ratio, mesh angles and filament ratios on the development of unsteady hydrodynamics. Energy loss analysis was also conducted based on specific power consumption generated by different spacer designs in the spiral wound membrane channel. Taking into account the presence of unsteady hydrodynamics, the influence of unsteady hydrodynamics on the development of concentration polarization was studied through wall shear stress analysis.

Based on the detail analysis on the hydrodynamics and permeation properties in the spacer filled SWM feed channel, the design and optimization of feed spacer were carried out in the subsequent study. Under current work, spacer design parameters

consisted of spacer filament geometry, mesh length ratio, mesh angles and spacer filament ratio. These design parameters were optimized in term of concentration polarization factor and specific power consumption. The desired criterion for optimum feed spacer's designs depends on the ability of the feed spacer to generate the lowest concentration factor under the specific range of power consumption.

In order to further confirm the validity of current optimum spacer designs, experimental validation and performance comparison for optimum spacer were conducted. Under experimental validation, hydrodynamics and permeation properties for the simulated optimum spacer filled membrane channel were verified based on experimental channel pressure drop and permeation flux. Besides, the performance of the optimized spacer was compared with other spacers (with different designs) in terms of permeation flux and observed rejection to further validate the optimum designs.

1.8 Organization of the thesis

This thesis consists of six chapters. In Chapter One (Introduction), a brief introduction about different types of membrane modules and the world market demand on membrane module especially spiral wound membrane (SWM) was given. The advantages of spiral wound membrane module were also highlighted through the comparison with other types of membrane module. This chapter also included the problem statements that provide some basis and rationale to identify the research direction to be followed in this study. Besides, the specific objectives of the present study were elaborated in detail together with the scopes of the current study to be covered. The organization of the contents of this thesis was also given in the last section of this chapter.

Chapter Two (Literature Review) reviewed the detail design, construction material for spiral wound membrane module (SWM). Besides, concentration polarization and fouling problem in the SWM coupled with the solutions for these problems were discussed in this chapter. This chapter also demonstrated detail description about the function and the design parameters for feed spacer. Then, the existing design methods for feed spacer which carried out by others researchers in their published literature and patents were elaborated. In the final part of this chapter, a summary was given to exhibit the uniqueness of current study as compared to other similar studies reported in the literature.

Chapter Three (Materials and Methods) was subdivided into two parts which were the modeling & simulation method and the experimental method. In the earlier part of the modeling and simulation method, discretization and solution methods for the governing equations were included. Next, permeation properties modeling, simulation approach, boundary condition, simulation condition, computational grid optimization and model validation approach were elaborated. In the experimental method, detail elaboration about the experimental set-up, material used and experimental procedures together with analytical method were incorporated in final part of this chapter.

Chapter Four (Results and Discussions) which is the main body of this thesis was outlined by three main sections. The first section discussed on the hydrodynamics and permeation properties in the narrow membrane channel. In order to estimate the concentration polarization accurately, permeation properties were integrated in the commercial CFD simulator for simulating the hydrodynamics and permeation properties in narrow empty membrane channel. This section also demonstrated the validation for the integrated CFD model and studied the influence of permeation flux on concentration polarization factor prediction. With the predicted concentration

polarization factor, the effect of feed Reynolds number, transmembrane pressure and different solutes on the development of concentration polarization were studied and discussed under this section. The capability of current integrated CFD model was extended to second section to study the hydrodynamics and permeation properties for the spacer filled SWM feed channel. In this section, the integrated CFD model for the spacer filled membrane channel was validated in term of hydrodynamics and permeation properties. After the model validation, unsteady hydrodynamics analysis was conducted for the spacer filled SWM feed channel. Besides, energy loss in the different spacers filled SWM feed channel was also determined using specific power consumption. Taking into account the presence of unsteady hydrodynamics, the influence of unsteady hydrodynamics on the development of concentration polarization factor was studied based on wall shear stress analysis. In the final section, design and optimization of feed spacer approaches were carried out based on the earlier analysis on the hydrodynamics and permeation properties in the spacer filled SWM feed channel. The feed spacer design parameters for current study consist of spacer filament geometry, mesh length ratio, mesh angles and spacer filament ratio. These design parameters were optimized in term of concentration polarization factor and specific power consumption. The optimized feed spacer model was validated experimentally and its performance was compared with other spacers with different designs in this section.

Chapter Five (Conclusions and Recommendations) contains the main conclusion of the current study. This chapter was written in the form of paragraph which discussing the conclusion based on the measurable objectives of this study. In the second part of this chapter, it consists of a list of recommendations for future studies in this related field.

CHAPTER 2

LITERATURE REVIEW

This chapter reviews the detail construction and material of spiral wound membrane module (SWM). Concentration polarization and fouling problem in the SWM coupled with the solutions for these problems were discussed in this chapter. This chapter also gives detail description about the function and design parameters for feed spacer. Then, the existing design methods for feed spacer which have been carried out by others researchers in their published literature and patents were elaborated. In the final part of this chapter, a summary was given to exhibit the uniqueness of current study as compared to other similar studies reported in the literature.

2.1 Construction and material of spiral wound membrane module

Spiral wound membrane (SWM) envelope/leaf consists of 2 flat sheet membranes which are sealed on three edges of a permeate spacer. Figure 2.1 depicts a schematic diagram for a membrane envelope. The fourth open edge is attached to the perforated permeate tube (refer to Figure 2.2). A permeate spacer is a material which create the permeate channel in the membrane envelope and direct the liquid flow of permeate solution to the permeate tube. Meanwhile, a feed spacer or sometimes known as retentate spacer, is placed on either side of the membrane envelope and wounded with the membrane leaf around the central tube (Schafer *et al.*, 2005). Important parts for the spiral wound membrane in a pressure vessel are illustrated in Figure 2.3.

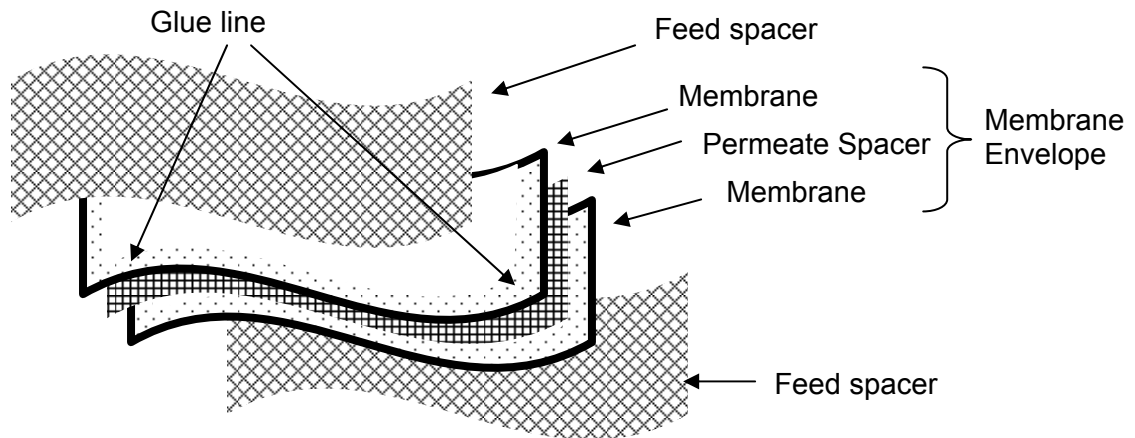


Figure 2.1: Membrane envelope (leaf)

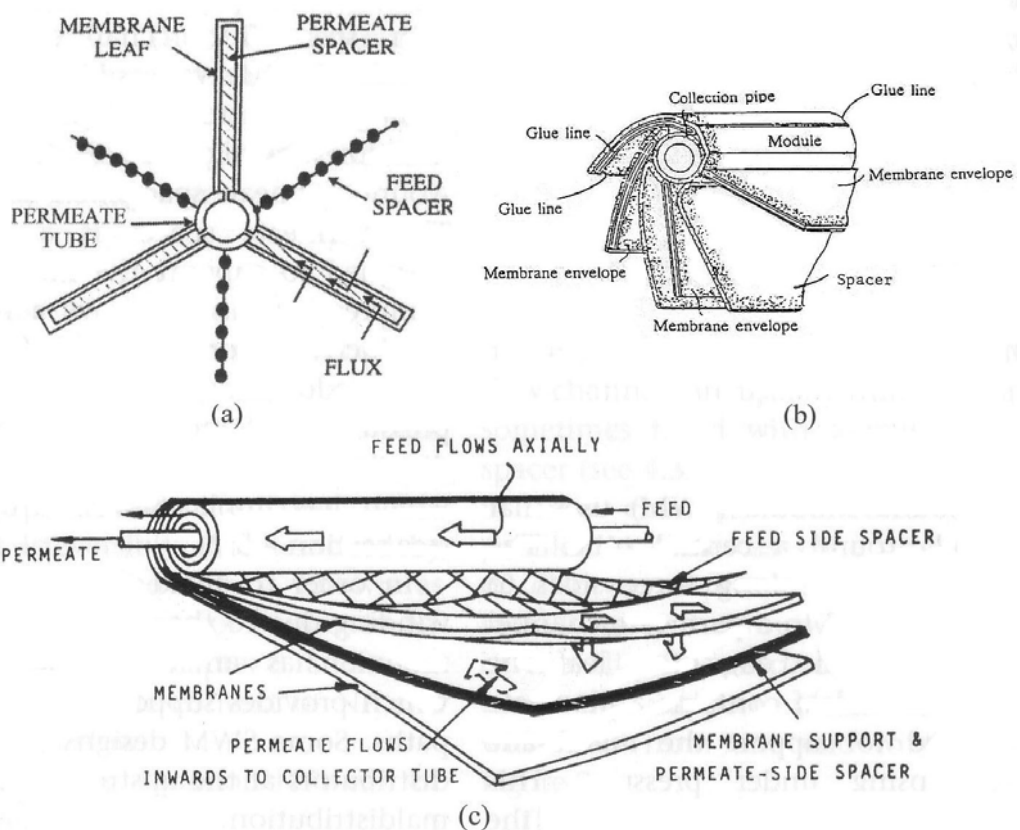


Figure 2.2: Spiral wound module: (a) basic element; leaves connected to a permeate tube, feed spacers between leaves; (b) leaves wound around permeate tube; (c) flows paths in SWM (Schafer *et al.*, 2005).

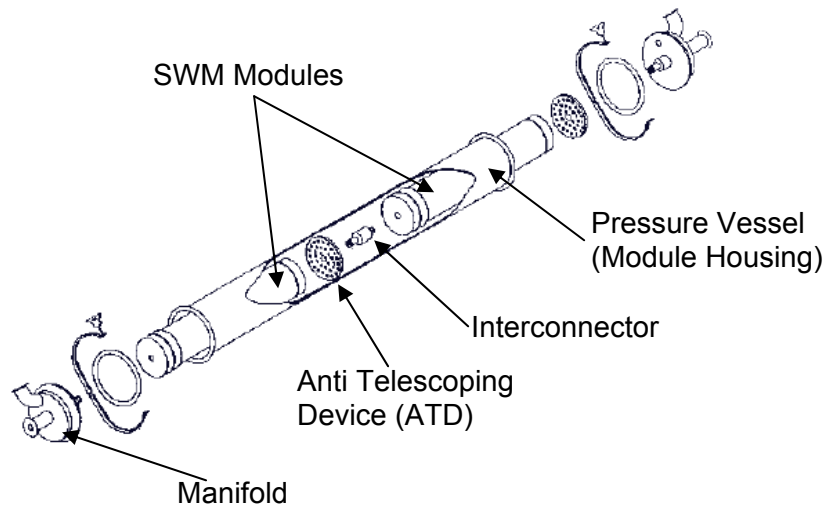


Figure 2.3: Important parts for spiral wound membrane in pressure vessel (Dow Water Solutions, 2007)

2.1.1 Permeate collection tube

The permeate collection tube is the center of the element which membrane leaves, permeate spacer and feed spacer are wound. This component is also known as center tube. It is perforated to allow the permeate flow spirally through the permeate spacer to the center of the element. The center tube provides structural strength to the element, as well as integrity toward thermal and chemical impact from the working environment (Schafer *et al.*, 2005). The common materials for the center tube are tabulated in Table 2.1.

Table 2.1: Material for permeate collection tube (Dow Water Solutions, 2007)

Material	Application
Noryl/ABS	Low pressure, ambient temperature environments with few chemical compatibility problems.
PVC	High pressure seawater application. (Inexpensive)
Polysulfone	Wider temperature and pH range with chemical resistant required environment.
Aluminum	Extremely high pressure environment.
Stainless Steel	Extremely high pressure environment with chemical resistant required environment.

2.1.2 Permeate spacer

The permeate spacer is a sheet of material inserted between the backsides of the membranes, forming a membrane envelope to promote the flow of permeate towards the center tube for discharge at the ends of the pressure vessel. The permeate spacer material must be able to withstand the pressure of operation without collapsing and blocking the flow, and the surface of the permeate spacer must be smooth to prevent intrusion of the membrane backing material into the permeate spacer. A polyester knit tricot stiffened with polymeric materials is used for normal operating pressures up to 600 psi (40.8 bar). At pressure up to 1500 psi (102 bar), combinations of tricot and other polymeric materials are used. Under extreme conditions of pressure, temperature or aggressive environments, various patterns of a metallic web or netting can be used (Lien, 1989).

2.1.3 Feed Spacer

Unlike permeate spacer, feed spacer plays an important role in membrane systems referring to problems of mass transfer, homogenizing and mixing behaviour. In spiral wound modules, these spacers have several functions as supporting nets and as turbulence promoters to increase mass transfer rates and reduce fouling layers (Fakova, 1991, Millward *et al.*, 1995; Zimmerer and Kottke, 1996; Sablanli *et al.*, 2002; Gimmerlshtein and Semiat, 2005; Auddy *et al.*, 2004). Plate 2.1 shows the photographic view of a commercial feed spacer. Various types of feed spacer are currently available in the market due to the wide-ranging of feed conditions such as high viscosity, suspended solids, high temperature, and presence of fouling species, and precipitation or crystal formation (Fulk, 1989; Feimer, 1994). The geometries and configuration of the feed spacer determine its suitability and performance in particular applications. The most common types of feed spacer that varies in term of configuration include diamond pattern spacer, parallel pattern spacer and corrugated